Quantum-Well Bound States in Graphene Heterostructure Interfaces

Zhongwei Dai (代中伟),[1,*] Zhaoli Gao,[2,4] Sergey S. Pershoguba,[3] Nikhil Tiwale,[1] Ashwanth Subramanian,[5] Qicheng Zhang,[2] Calley Eads,[1] Samuel A. Tenney,[1] Richard M. Osgood,[6] Chang-Yong Nam,[1,5] Jiadong Zang,[3] A. T. Charlie Johnson,[2] and Jerzy T. Sadowski[1,†]

[1]*Center for Functional Nanomaterials, Brookhaven National Laboratory, Upton, New York 11973, USA*
[2]*Department of Physics and Astronomy, University of Pennsylvania, Philadelphia, Pennsylvania 19104, USA*
[3]*Department of Physics and Astronomy and Materials Science Program, University of New Hampshire, Durham, New Hampshire 03824, USA*
[4]*Department of Biomedical Engineering, The Chinese University of Hong Kong, Hong Kong, China*
[5]*Department of Materials Science and Chemical Engineering, Stony Brook University, Stony Brook, New York 11794, USA*
[6]*Department of Electrical Engineering, Columbia University, New York, New York 10027, USA*

(Received 19 February 2021; accepted 24 June 2021; published 20 August 2021)

We present experimental evidence of electronic and optical interlayer resonances in graphene van der Waals heterostructure interfaces. Using the spectroscopic mode of a low-energy electron microscope (LEEM), we characterized these interlayer resonant states up to 10 eV above the vacuum level. Compared with nontwisted, AB-stacked bilayer graphene (AB BLG), an ≈0.2 Å increase was found in the interlayer spacing of 30° twisted bilayer graphene (30°-tBLG). In addition, we used Raman spectroscopy to probe the inelastic light-matter interactions. A unique type of Fano resonance was found around the D and G modes of the graphene lattice vibrations. This anomalous, robust Fano resonance is a direct result of quantum confinement and the interplay between discrete phonon states and the excitonic continuum.

DOI: 10.1103/PhysRevLett.127.086805

Resonant interference of confined waves can strongly alter wave motion. Under certain configurations, exotic bound states embedded in the continuum may emerge [1]. Confinement of waves is ubiquitous in nature, and is often found at an interface, or on a surface [2,3], where symmetry breaking is unavoidable and the role of boundary conditions in wave motion becomes significant. In the quantum regime, quantum confinement effects emerge when the material system's geometrical size is reduced to be comparable to an electron's de Broglie wavelength [4–7]. The interference of electron waves scattered by different boundaries or interfaces leads to quantized discrete energy levels, forming standing-wavelike eigenstates, or quantum well (QW) bound states in epitaxial thin films [5,8]. These QW states modulate electronic behavior periodically at all energy scales, including electronic states around the Fermi level and electron-phonon coupling [5,8]. Previous reports show that the QW states have a significant impact on electronic spin [4,6,7], superconductivity [5], and the electron mean free path [9].

In the case of graphene-based material systems, QW states form due to a resonant interlayer multiple scattering. The QW states in few-layer graphene appear as layer number–dependent quantized electronic bands in both occupied and unoccupied energy levels. The discrete unoccupied electronic states that are above the vacuum level can be captured by low-energy electron reflectivity (LEER) measurements that use a coherent low-energy (typically less than 10 eV) electron beam. A LEER spectrum obtained from N layers of graphene usually has $N-1$ or N minima, depending on the substrate interaction [9–11]. In particular, the LEER spectrum of single-layer graphene (SLG) transferred on a substrate (such as thermally processed SiO_2) usually has no apparent minimum, due to inhomogeneity in the supporting substrate [12]. In bilayer graphene (BLG) systems, the LEER spectra usually have one minimum located around 2.6 eV above the vacuum level. This energy state is a manifestation of interlayer resonant multiple scattering, and it is localized in between the graphene layers. Discovery of superconductivity in a twisted "magic-angle" bilayer graphene system [13] has stimulated renewed discussions about weak van der Waals interlayer interaction in layered material systems. Wu *et al.* proposed a phonon-mediated superconductivity mechanism which highlighted the interlayer electron-phonon coupling [14]. Besides the commensurate small twist-angle BLG, an incommensurate 30° twisted bilayer graphene (30°-tBLG) has recently emerged as a promising system to study quasicrystallinity [15,16] and exotic localization phenomena [17].

In this report, we present results of a comprehensive investigation of the interlayer resonances and quantum confinement effects in two types of unconventional graphene interfaces: graphene-TiO_x heterostructure interface and graphene-graphene interface in 30°-tBLG [15,16]. We have used two fundamentally different elemental particles

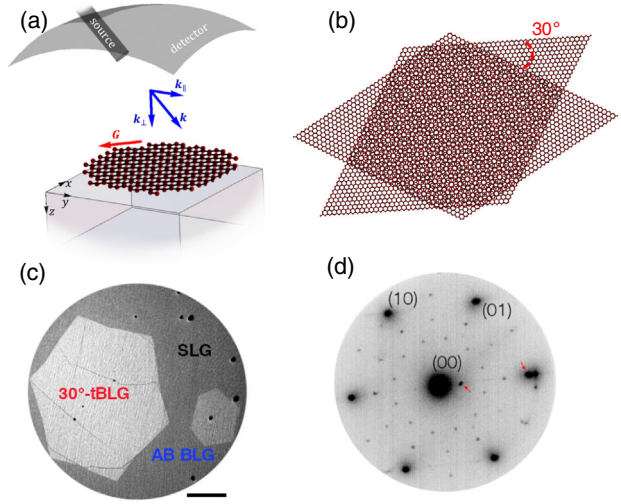

FIG. 1. Low-energy electron microscopy of graphene grown via CVD on a Ni–Cu gradient alloy foil. (a) Schematics of electron and photon scattering experimental setup. (b) Atomic model of the dodecagonal pattern formed by the 30°-tBLG crystal structure. (c) Bright-field LEEM image of a typical sample area, incident electron energy $E = 5.6$ eV; the scale bar is 5 μm. (d) μ-LEED on a 30°-tBLG area taken at an electron energy of $E = 42$ eV.

as probes. First, we used electrons (fermions) at very low energy (0–10 eV) in a back-scattering setup in a low-energy electron microscope (LEEM) to probe the electronic resonances. Furthermore, we used photons (bosons, $E = 2.3$ eV, $\lambda = 532$ nm) for inelastic photon-electron scattering in a confocal Raman spectromicroscope to probe electron-phonon coupling. The schematic of the experimental setup for electron and Raman scattering is shown in Fig. 1(a).

The states detected by LEER correspond to electronic states above the vacuum level in the continuum energy range [18]. The local conduction band electronic structure can be extracted with a high spatial resolution, up to a few nanometers [18]. An electron traveling in a free space, with energy $E_e = (p^2/2m_e)$, can be described by a plane wave function, $\psi(\vec{r}) = e^{i(\vec{p}\cdot\vec{r}-Et)/\hbar}$. Using de Broglie's equation $\lambda_e = (h/p)$, an electron with energy of 3 eV has a wavelength of about 7 Å, which is comparable to the interlayer spacing in few-layer graphene (≈3.34 Å in AB-stacking configuration [19]). Under conditions of normal incidence, an interlayer resonance forms when the interlayer spacing d satisfies $2d = n\lambda$.

Thirty-degree twisted bilayer graphene was synthesized by chemical vapor deposition (CVD) using a Ni–Cu gradient alloy foil as the substrate following the recipe reported in a previous study [20]. The as-grown graphene samples were investigated using an aberration-corrected LEEM [21]. In the LEEM bright-field mode, an image of the surface is formed by elastically back-scattered electrons, upon normal incidence of a coherent electron beam. The atomic crystal 30°-tBLG is shown in Fig. 1(b). Figure 1(c) shows a bright-field LEEM image of a 30 μm sample area of as-grown 30°-tBLG, accompanied by an AB-stacked bilayer graphene (AB BLG) area, and an SLG. Three different types of the 2D interfacial material systems are readily available for investigation under the same experimental conditions: 30°-tBLG graphene plane interface, the AB BLG interface, and the SLG-substrate interface. Distinct reflectivity contrasts were captured between 30°-tBLG and AB BLG, indicating a difference in the electronic structure between the two systems. Local diffraction experiments were conducted *in situ* using the microspot low-energy electron diffraction with a 1.5 μm selected-area aperture. Figure 1(d) shows a diffraction pattern acquired on the 30°-tBLG. Apart from the specular spot in the center, the strongest spots are first order diffraction beams due to graphene honeycomb lattice, and are indexed as (10) and (01). A second set of first order diffraction spots rotated by 30° is from the underlying second layer of graphene. The inside, weaker 12 discrete diffraction spots are the fractional order beams formed due to elastic interlayer scattering. Extra spots that are marked by red arrows originate from the substrate surface. Our LEED data are consistent with a recent report on the quasicrystalline perspective of 30°-tBLG grown on SiC [15].

LEER experiments were conducted at room temperature on the graphene transferred onto the TiO_x substrates developed for the QPress project at the Center for Functional Nanomaterials, BNL. The 3.5 nm thick TiO_x films were grown by atomic layer deposition on the surface of a 300 nm thick SiO_2 on a Si wafer and annealed in forming gas (4% H_2/Ar_2) to form an oxygen vacancy–rich film. The ultrathin TiO_x film is semiconducting and serves two main purposes: (i) to provide sub nm–level flatness to support a graphene system and enable interface interactions and (ii) to induce effective electron wave or light wave trapping to enable robust interactions through proximity effects. A high-resolution transmission electron microscope image of a typical TiO_x film is shown in Supplemental Material [22], Sec. I, Fig. S1. Detailed synthesis, graphene transfer methods [20], and electronic transport characterization of the TiO_x thin film are reported elsewhere [23].

Nanoscale local-area LEER curves were simultaneously acquired by conducting dynamical measurements, in which the incident electron energy is tuned, and the corresponding reflected electron intensity is recorded in the form of images of the surface, known as LEEM-*IV* [10,24]. Figure 2(c) contains the LEEM-*IV* spectra obtained from the three different types of sample areas shown in Fig. 2(a). Figure 2(b) shows the side view of the investigated graphene interfaces. Two distinct minima were observed on both, 30°-tBLG and AB BLG [marked by grey vertical lines in Fig. 2(c)]. The energy difference between the two minima ΔE is a result of energy state splitting due to a

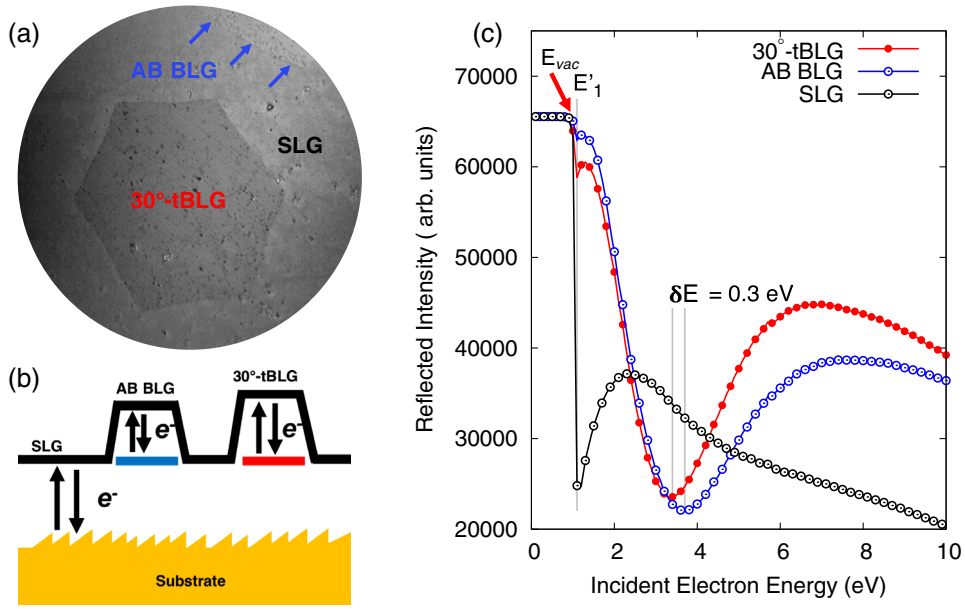

FIG. 2. Dynamical low-energy electron reflectivity of graphene systems on TiO_x substrate. (a) Bright-field LEEM image of a typical 30°-tBLG sample on TiO_x, $E = 2.3$ eV, scale bar is 5 μm. (b) Schematics of side view of presented graphene interface material system. (c) LEEM-*IV* spectra of 30°-tBLG, AB BLG, and SLG samples on TiO_x.

formation of interlayer electron resonant scattering state, and it is a direct measurement of the interlayer bonding energy in BLG systems. It can be associated with the nearest-neighbor hopping integral t, by $\Delta E = 2t$ [10]. For AB bilayer stacking, we measured $\Delta E_{\mathrm{AB}} = 2.6$ eV, which is consistent with the calculated value for the free-standing scenario [11]. For the 30°-tBLG, $\Delta E_{\mathrm{tBLG}} = 2.3$ eV, which is about 0.3 eV smaller than $\Delta E_{\mathrm{AB}} = 2.6$ eV. This $\delta E = 0.3$ eV energy shift due to a simple interlayer twist is remarkable, and 1 order of magnitude bigger than previously thought [25]. Coincidentally, this δE is the same value as the interlayer hopping energy, $t_\perp$ [26].

The interlayer resonant electron energy is directly associated with the wavelength of the electron wave packet in the 2D interfacial confinement space. Using the de Broglie's equation $\lambda_e = (h/p)$, we write the standing wave condition as $2d = n\lambda_e$, with integer n. The experimentally relevant resonant mode corresponds to $n = 1$ and $d = (\lambda_e/2)$. The above analysis immediately yields the direct relation between the experimentally observed dip energy difference ΔE and interlayer spacing d in bilayer graphene systems: $\Delta E = (h^2/8m_e) \times (1/d^2)$ or

$$d \propto \Delta E^{-\frac{1}{2}}, \tag{1}$$

which produces $(d_{\mathrm{tBLG}}/d_{\mathrm{AB}}) = \sqrt{(\Delta E_{\mathrm{AB}}/\Delta E_{\mathrm{tBLG}})} \approx 1.06$. Based on the simple estimate above, we find that the interlayer spacing of 30°-tBLG is increased by about 6%, compared with the AB BLG. Assuming an AB BLG interlayer spacing of 3.34 Å, this means ≈0.2 Å increase in the 30°-tBLG interlayer spacing. In the BLG systems, the interlayer spacing and electronic structure are strongly correlated [27]. The observed interlayer bonding energy difference between AB BLG and 30°-tBLG may have a deep impact on the system's electronic properties and its electron-quasi-particle interactions [28,29].

In the SLG-TiO_x LEEM-*IV* spectrum, shown in Fig. 2(c), there is a pronounced sharp minimum having a Fano-asymmetry shape, which has not been previously observed. This result indicates a formation of a robust SLG-TiO_x interface electron resonant state. This state is only about 0.1 eV above the vacuum energy level, as determined by the energy difference of the first minimum and onset drop of the reflected intensity. The Fano shape may indicate the existence of continuum gradient resonant electronic states [29]. The origin of this phenomenon could be due to the formation of a gradient electric field in the interface space induced by a high concentration of confined charges, which are similar to previously reported epitaxially grown graphene-substrate interfaces [15,28]. It is worth noting that achieving a well-defined electronic interaction between the transferred graphene and substrate without damaging the graphene's intrinsic properties is critical for the scaling up and design of next generation graphene-based electronic and optoelectronic devices.

A 1D quantum potential well model can be used to illustrate the observed interlayer resonances. Each graphene plane is modeled as an individual, Dirac delta function potential with scattering strength $v_0^{(1)}$ and $v_0^{(2)}$ for the top and bottom graphene layers, respectively. The TiO_x substrate is modeled as a constant scalar scattering potential normal to the surface v_{sr} (see Supplemental Material [22], Sec. II, for details). A comparison of our analysis with the experimental LEEM spectra seen in

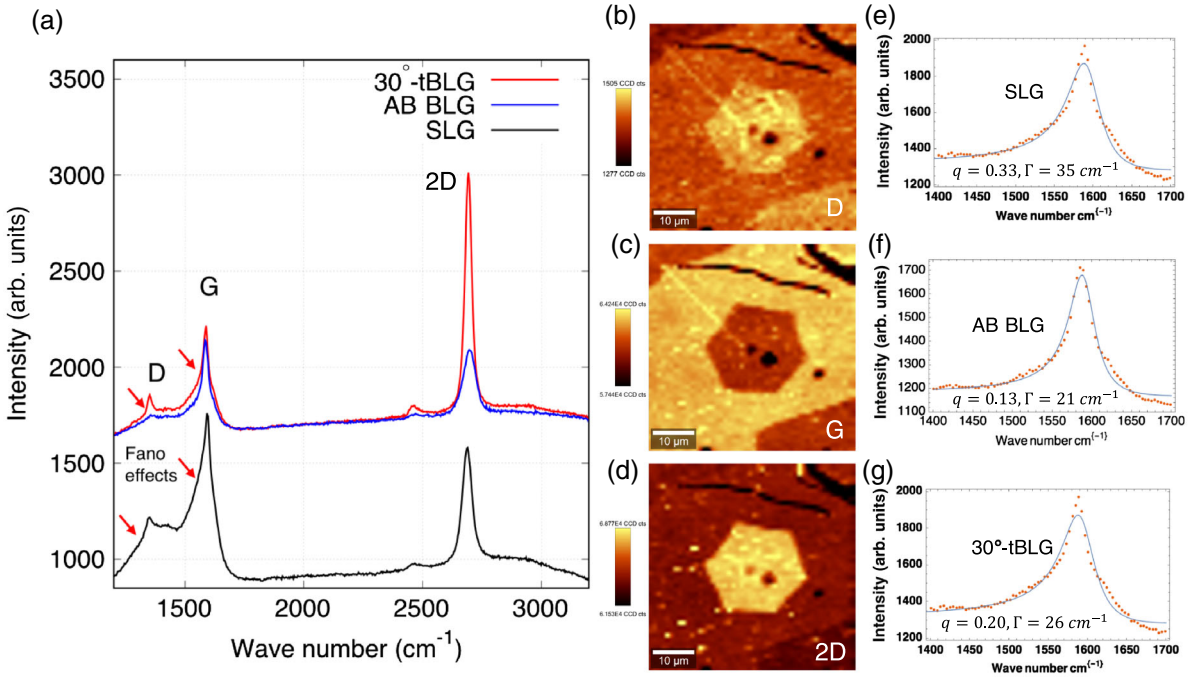

FIG. 3. (a) Raman spectrum of a transferred SLG, AB BLG, and 30°-tBLG on TiO_x substrate. (b)–(d) Scanning Raman image using integrated peak intensity centered around D peak, G peak, and 2D peak, respectively; integration window is 100 cm^{-1}. (e)–(g) Fano model fitting of G peak for SLG, AB BLG, and 30°-tBLG, respectively.

Fig. 2(c) allows us to draw several conclusions about the system: (i) The sharp dip pinned to the high-energy side of the LEEM reflectivity plateau is observed in both monolayer and bilayer systems. The dip occurs due to the $\propto \sqrt{E - v_{sr}}$ terms in the reflectivity formula (see Supplemental Material [22], Sec. II) and does not have a conventional Lorentzian profile. The sharpness of the dip is very sensitive to the quality of the graphene-TiO_x interface, and it attests to an electronically sharp and well-defined interface. (ii) The function of the amorphous TiO_x substrate can be approximated as a well-defined out-of-plane scalar electric potential $v_{sr} = 0.95$ eV during a scattering event. (iii) We find that the scattering potential of graphene is negative, i.e., $v_0 < 0$. That sign is consistent with an attractive image potential between an incoming electron and a graphene plane. (iv) For the bilayer systems, nonvanishing reflectivity $|r(E_{res})|^2 \neq 0$ at resonances E_{res} indicates nonequal scattering potentials $v_0^{(1)} \neq v_0^{(2)}$ [30]. Quantified scattering potential on each plane can be found in the Supplemental Material [22], Sec. II. The nonequal scattering potential could indicate a charge redistribution between the graphene layers in both BLG systems, which is also a result of symmetry breaking, due to the TiO_x induced out-of-plane electric field. This is similar to the gating effects in BLG which result in the formation of a gap in the electronic spectrum [31]. Comparison of the calculated electron reflectivity spectra with the experimental data shows good agreement (see Fig. S2 in the Supplemental Material [22], Sec. II, which includes Refs. [30–33]).

The external field induced by the substrate can have a great impact on graphene's properties, due to a proximity effect and symmetry breaking [34,35]. In the SLG scenario, Anderson localization-delocalization may happen in an external electric field [35]. In case of a bilayer, an external field would introduce charge transfer between layers, leading to a formation of excitons [34]. If the exciton's lifetime is long enough, coupling with phonons can become significant, giving rise to Fano resonance in the inelastic Raman scattering process.

To examine this process, we explored in more detail the electron-phonon interactions in the graphene bilayer systems, using a confocal micro-Raman spectroscopy with a 532 nm (~2.3 eV) excitation. For consistency, we have located the same sample area as was investigated in the LEEM-*IV* experiments. In the Raman spectrum shown in Fig. 3, we identified three peaks: (i) 2D peak at around $q = 2690$ cm^{-1}, (ii) G peak centered around $q = 1600$ cm^{-1}, and (iii) D peak centered around $q = 1349$ cm^{-1}. Comparing the Raman spectrum of 30°-tBLG with AB BLG, 2D peak intensity is strongly enhanced, by approximately 4 times. We attribute this enhancement to the increased probability of intervalley double resonance scattering caused by replicated and mirrored Dirac cones in the Brillouin zone in 30°-tBLG [15]. For the SLG on TiO_x substrate, the Raman spectrum shows a distinct high-intensity D peak. The D peak does not originate from the defects in the graphene sample itself. The graphene samples are pristine, as the Raman spectrum

of graphene transferred to a conventional 300 nm SiO_2 shows negligible intensity around $q = 1349\ \mathrm{cm}^{-1}$ [Supplemental Material [22], Sec. I, Fig. S3(a)]. Also, the D peak does not originate from the TiO_x substrate, as shown in the Raman spectrum of bare TiO_x in the Supplemental Material [22], Sec. I, Fig. S3(b). Previously, it was believed that the D peak in graphene was from localized electronic defect states coupled with a zone-center phonon mode of graphene [36]. In this electron-phonon coupling process, only energy is transferred while momentum is not exchanged [36]. The D peak was usually observed around defects, or boundaries of graphene [36]. However, our experiments show that emergence of the D peak is due to the interface interaction in the SLG-TiO_x heterostructure. Specifically, the defect electronic states at the surface of the TiO_x substrate couple with the graphene lattice vibrational modes. Moreover, the G peak of SLG-TiO_x shows enormous intensity, also having a Fano-shape asymmetry. The intensity of the G peak is even larger than the SLG 2D peak. On a conventional 300 nm SiO_2 substrate, the Raman spectrum of SLG shows a much smaller G peak intensity compared with the 2D peak [see Supplemental Material [22], Fig. S3(a)]. The G peak in SLG-TiO_x also shows a significant asymmetry feature with a broad peak width ($\sim 100\ \mathrm{cm}^{-1}$). Similar Fano effects around the G peak have been reported by IR spectroscopy, and were attributed to the graphene zone-center phonon mode (0.2 eV) coupled with continuum electronic states in the system [37]. However the origin of the continuum electronic states was not elucidated, and the Fano-shaped peak width only spanned $\sim 10\ \mathrm{cm}^{-1}$.

In summary, we have studied the electronic and optical wave interferences and resonances in the unique, high quality, large area SLG-TiO_x and dodecagonal 30°-tBLG interface systems. The LEED patterns show a strong interlayer scattering and a 12-fold rotational symmetry in as-grown 30°-tBLG. The energy of the interlayer electronic resonant state in 30°-tBLG was found to be 0.3 eV lower compared with the well-known AB BLG. This result indicates that the interlayer spacing in 30°-tBLG is about 6%, or ≈ 0.2 Å greater than that of AB BLG. The increase of the interlayer spacing in 30°-tBLG may have a profound impact on its electronic properties, such as smaller interlayer bonding energy, which makes 30°-tBLG more susceptible to external perturbation. Both the LEEM-*IV* and Raman results consistently show a strong graphene-graphene interface interaction resulting from the continuum electronic defect states coupled with phonon, or plasmon; thus, the 30°-tBLG interface presents unique interlayer resonant interaction, in which interlayer scattering is greatly enhanced.

We have also shown that the SLG-TiO_x interface hosts multiple types of Fano resonances in both electron- and photon-matter interactions. In the electron case, SLG-TiO_x functions as a waveguide (graphene) with a perfect reflecting mirror (TiO_x). The entire system reduces to a 1D Fabry-Perót resonator. It has a sharp Fano resonance at energy just 0.1 eV above the vacuum level [2]. Upon visible photon excitation, interlayer exciton forms and interacts with phonons, manifesting itself as Fano-shaped peaks in the Raman scattering process, around the G and D mode of graphene. In the case of SLG-TiO_x, waves are confined within the interface between two individual surfaces.

This research used resources from the Center for Functional Nanomaterials and the National Synchrotron Light Source II, which are U.S. Department of Energy (DOE) Office of Science facilities at Brookhaven National Laboratory, under Contract No. DE-SC0012704. Z. G., Q. Z., and A. T. C. J. acknowledge support from the National Science Foundation through MRSEC DMR-1720530 and EAGER 1838412. Z. G. acknowledges support from the Research Grant Council of Hong Kong SAR (Project No. 24201020) and a Direct Grant from The Chinese University of Hong Kong (Project No. 4055121). J. Z. and S. P. acknowledge financial support by the U.S. Department of Energy (DOE), Office of Science, Basic Energy Sciences (BES) under Award No. DE-SC0020221. We thank Kim Kisslinger for assistance with the TEM characterization. We acknowledge useful discussions with X. Tong, J.-X. Yu, M. Lu, and Y. J. Shin.

*Corresponding author.
zhongwei@bnl.gov
†Corresponding author.
sadowski@bnl.gov

[1] J. V. Neumann and E. Wigner, On some peculiar discrete eigenvalues, Phys. Z **30**, 465 (1929).

[2] S. Weimann, Y. Xu, R. Keil, A. E. Miroshnichenko, A. Tünnermann, S. Nolte, A. A. Sukhorukov, A. Szameit, and Y. S. Kivshar, Compact Surface Fano States Embedded in the Continuum of Waveguide Arrays, Phys. Rev. Lett. **111**, 240403 (2013).

[3] A. G. Every and A. A. Maznev, Elastic waves at periodically-structured surfaces and interfaces of solids, AIP Adv. **4**, 124401 (2014).

[4] R. Zdyb and E. Bauer, Spin-Resolved Unoccupied Electronic Band Structure from Quantum Size Oscillations in the Reflectivity of Slow Electrons from Ultrathin Ferromagnetic Crystals, Phys. Rev. Lett. **88**, 166403 (2002).

[5] Y. Guo, Y. F. Zhang, X. Y. Bao, T. Z. Han, Z. Tang, L. X. Zhang, W. G. Zhu, E. G. Wang, Q. Niu, Z. Q. Qiu, J. F. Jia, Z. X. Zhao, and Q. K. Xue, Superconductivity modulated by quantum size effects, Science **306**, 1915 (2004).

[6] C. Berger, X. Wu, N. Brown, C. Naud, X. Li, Z. Song, D. Mayou, T. Li, J. Hass, a. Marchenkov, E. H. Conrad, P. N. First, and W. a. De Heer, Electronic Confinement and coherence in patterned epitaxial graphene, Science **312**, 1191 (2006).

[7] Y. Z. Wu, A. K. Schmid, and Z. Q. Qiu, Spin-Dependent Quantum Interference from Epitaxial MgO Thin Films on Fe(001), Phys. Rev. Lett. **97**, 217205 (2006).

[8] J. J. Paggel, T. Miller, and T.-C. Chiang, Quantum-well states as Fabry-Perót modes in a thin-film electron interferometer, Science **283**, 1709 (1999).

[9] D. Geelen, J. Jobst, E. E. Krasovskii, S. J. Van Der Molen, and R. M. Tromp, Nonuniversal Transverse Electron Mean Free Path through Few-layer Graphene, Phys. Rev. Lett. **123**, 086802 (2019).

[10] H. Hibino, H. Kageshima, F. Maeda, M. Nagase, Y. Kobayashi, and H. Yamaguchi, Microscopic thickness determination of thin graphite films formed on SiC from quantized oscillation in reflectivity of low-energy electrons, Phys. Rev. B **77**, 075413 (2008).

[11] N. Srivastava, Q. Gao, M. Widom, R. M. Feenstra, Shu Nie, K. F. McCarty, and I. V. Vlassiouk, Low-energy electron reflectivity of graphene on copper and other substrates, Phys. Rev. B **87**, 245414 (2013).

[12] A. Locatelli, K. R. Knox, D. Cvetko, T. O. Mente, M. A. Niño, S. Wang, M. B. Yilmaz, P. Kim, R. M. Osgood, and A. Morgante, Corrugation in exfoliated graphene: An electron microscopy and diffraction study, ACS Nano **4**, 4879 (2010).

[13] Y. Cao, V. Fatemi, S. Fang, K. Watanabe, T. Taniguchi, E. Kaxiras, and P. Jarillo-herrero, Unconventional superconductivity in magic-angle graphene superlattices, Nature (London) **556**, 43 (2018).

[14] F. Wu, A. H. MacDonald, and I. Martin, Theory of Phonon-Mediated Superconductivity in Twisted Bilayer Graphene, Phys. Rev. Lett. **121**, 257001 (2018).

[15] S. J. Ahn, P. Moon, T. H. Kim, H. W. Kim, H. C. Shin, E. H. Kim, H. W. Cha, S. J. Kahng, P. Kim, M. Koshino, Y. W. Son, C. W. Yang, and J. R. Ahn, Dirac electrons in a dodecagonal graphene quasicrystal, Science **361**, 782 (2018).

[16] W. Yao, E. Wang, C. Bao, Y. Zhang, K. Zhang, K. Bao, C. K. Chan, C. Chen, J. Avila, M. C. Asensio, J. Zhu, and S. Zhou, Quasicrystalline 30° twisted bilayer graphene as an incommensurate superlattice with strong interlayer coupling, Proc. Natl. Acad. Sci. U.S.A. **115**, 6928 (2018).

[17] M. J. Park, H. S. Kim, and S. B. Lee, Emergent localization in dodecagonal bilayer quasicrystals, Phys. Rev. B **99**, 245401 (2019).

[18] J. Jobst, J. Kautz, D. Geelen, R. M. Tromp, and S. J. Van Der Molen, Nanoscale measurements of unoccupied band dispersion in few-layer graphene, Nat. Commun. **6**, 8926 (2015).

[19] B. T. Kelly, *Physics of Graphite* (Applied Science, London, 1981).

[20] Z.Gao, Q. Zhang, C. H. Naylor, Y. Kim, I. H. Abidi, J. Ping, P. Ducos, J. Zauberman, M.-Q. Zhao, A. M. Rappe, Z. Luo, L. Ren, and A. T. Charlie Johnson, Crystalline bilayer graphene with preferential stacking from Ni–Cu gradient alloy, ACS Nano **12**, 2275 (2018).

[21] E. Bauer, *Surface Microscopy with Low-Energy Electrons* (Springer-Verlag, New York, 2014).

[22] See Supplemental Material at http://link.aps.org/supplemental/10.1103/PhysRevLett.127.086805 for expanded experimental data and details of theoretical modelling.

[23] N. Tiwale, A. Subramanian, Z. Dai, S. Sikder, J. T. Sadowski, and C.-Y. Nam, Large mobility modulation in ultrathin amorphous titanium oxide transistors, Commun. Mater. **1**, 94 (2020).

[24] P. W. Sutter, J. I. Flege, and E. A. Sutter, Epitaxial graphene on ruthenium, Nat. Mater. **7**, 406 (2008).

[25] T. Ohta, J. T. Robinson, P. J. Feibelman, A. Bostwick, E. Rotenberg, and T. E. Beechem, Evidence for Interlayer Coupling and Moiré Periodic Potentials in Twisted Bilayer Graphene, Phys. Rev. Lett. **109**, 186807 (2012).

[26] R. R. Nair, P. Blake, A. N. Grigorenko, K. S. Novoselov, T. J. Booth, T. Stauber, N. M. R. Peres, and A. K. Geim, Fine structure constant defines visual transparency of graphene, Science **320**, 1308 (2008).

[27] A. V. Rozhkov, A. O. Sboychakov, A. L. Rakhmanov, and F. Nori, Electronic properties of graphene-based bilayer systems, Phys. Rep. **648**, 1 (2016).

[28] A. Bostwick, T. Ohta, T. Seyller, K. Horn, and E. Rotenberg, Quasiparticle dynamics in graphene, Nat. Phys. **3**, 36 (2007).

[29] A. N. Grigorenko, M. Polini, and K. S. Novoselov, Graphene plasmonics, Nat. Photonics **6**, 749 (2012).

[30] I. Yanetka, On the transmission coefficient for the double δ-function potential, Acta Phys. Pol. A **97**, 1053 (2000).

[31] E. McCann, Asymmetry gap in the electronic band structure of bilayer graphene, Phys. Rev. B **74**, 161403(R) (2006).

[32] V. U. Nazarov, E. E. Krasovskii, and V. M. Silkin, Scattering resonances in two-dimensional crystals with application to graphene, Phys. Rev. B **87**, 041405(R) (2013).

[33] J. I. Flege and E. E. Krasovskii, Intensity-voltage low-energy electron microscopy for functional materials characterization, Phys. Status Solidi Lett. **8**, 463 (2014).

[34] T.-T. Tang, Y. Zhang, C.-H. Park, B. Geng, C. Girit, Z. Hao, M. C. Martin, A. Zettl, M. F. Crommie, S. G. Louie, Y. R. Shen, and F. Wang, A tunable phonon-exciton Fano system in bilayer graphene, Nat. Nanotechnol. **5**, 32 (2010).

[35] S. Kim and K. Kim, Anderson localization and delocalization of massless two-dimensional dirac electrons in random one-dimensional scalar and vector potentials, Phys. Rev. B **99**, 014205 (2019).

[36] A. C. Ferrari, J. C. Meyer, V. Scardaci, C. Casiraghi, M. Lazzeri, F. Mauri, S. Piscanec, D. Jiang, K. S. Novoselov, S. Roth, and A. K. Geim, Raman Spectrum of Graphene and Graphene Layers, Phys. Rev. Lett. **97**, 187401 (2006).

[37] J. M. Baranowski, M. Mozdzonek, P. Dabrowski, K. Grodecki, P. Osewski, W. Kozlowski, M. Kopciuszynski, and W. Strupinski, Observation of electron-phonon couplings and Fano resonances in epitaxial bilayer graphene, Graphene **02**, 115 (2013).